



OPEN ACCESS

RECEIVED

5 November 2016

REVISED

24 March 2017

ACCEPTED FOR PUBLICATION

6 April 2017

PUBLISHED

26 May 2017

Original content from this work may be used under the terms of the [Creative Commons Attribution 3.0 licence](#).

Any further distribution of this work must maintain attribution to the author(s) and the title of the work, journal citation and DOI.



PAPER

Pairwise entanglement and the Mott transition for correlated electrons in nanochains

Adam Rycerz

Marian Smoluchowski Institute of Physics, Jagiellonian University, Łojasiewicza 11, PL–30348 Kraków, Poland

E-mail: rycerz@th.if.uj.edu.pl**Keywords:** quantum entanglement, metal–insulator transition, electron correlations, nanoscopic systems

Abstract

Pairwise entanglement, calculated separately for charge and spin degrees of freedom, is proposed as a ground-state signature of the Mott transition in correlated nanoscopic systems. Utilizing the exact diagonalization—*ab initio*, for chains containing $N \leq 16$ hydrogenic-like atoms (at the half filling), we find that the vanishing of the nearest-neighbor charge concurrence indicates the crossover from a partly-localized quantum liquid to the Mott insulator. Spin concurrence remains nonzero at the insulating phase, showing that the decoupling of spin and charge degrees of freedom may manifest itself by wavefunctions entangled in spin, but separable in charge coordinates. At the quarter filling, the analysis for $N \leq 20$ shows that spin concurrence vanishes immediately when the charge-energy gap obtained from the scaling with $1/N \rightarrow 0$ vanishes, constituting a finite-system version of the Mott transition. Analytic derivations of the formulas expressing either charge or spin concurrence in terms of ground-state correlation functions are also provided.

1. Introduction

In 90 years after the seminal work by Schrödinger [1] analytical properties of quantum-mechanical wavefunctions describing hydrogenic-like atoms (or ions) continue to surprise. For instance, recent derivation of the Wallis formula for π by Friedmann and Hagen [2] refers to the variational principle and the correspondence principle, but also employs a counterintuitive fact that some variational approaches may truncate particular excited states of atoms with the same or better accuracy than the ground state (GS). This feature has direct analogs in many-electron hydrogenic systems and motivated the proposal of the exact diagonalization—*ab initio* method (EDABI) [3], which were recently used to discuss the influence of electron correlations on the metallization of solid hydrogen in a rigorous manner [4, 5]. Also, as a method putting equal footing on single- and multiparticle aspects of the correlated quantum states, EDABI seems to be a promising candidate for the theoretical tool capable of giving a better insight into the superconductivity mechanism in sulfur hydrides [6, 7] or into the magnetic moment formation in functionalized graphenes [8].

When considering a generic second-quantized Hamiltonian with both spin and charge degrees of freedom, a few numerical techniques can be regarded as exact ones; i.e., giving the desired correlation functions within the accuracy limited (in principle) by the machine precision only. These includes: exact diagonalization (ED) for relatively small systems [9], density matrix renormalization group (DMRG) for low-dimensional systems [10], and quantum Monte Carlo (QMC) for non-frustrated systems [11]. A separate class is outlined by variational approaches designed to treat one-dimensional (1D) atomic chains in the insulating phase [12]. Even though each of these methods provides us with detailed information about the closed-system GS, it is usually a challenging task to determine whether GS is insulating, metallic, or of a more complex nature [13]¹. This is primarily because standard GS signatures of the metal–insulator transition, such as a vanishing charge gap [14], are absent at any finite system size (quantified by the number of lattice sites N), but may appear only after the so-called finite-size scaling (with $1/N \rightarrow 0$), a procedure introducing systematic errors difficult to estimate in some cases.

¹ For the discussion of a recent controversy concerning the existence of a spin-liquid phase in the Hubbard model on the honeycomb lattice, see [13].

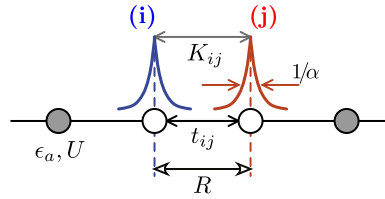


Figure 1. A system studied numerically (schematic). Hydrogenic-like atoms, containing 1s-type orbitals with their radii α^{-1} , are arranged linearly with the interatomic distance R . The Hamiltonian parameters, including the atomic energy ϵ_a , the intraatomic Coulomb integral U , the hopping integrals t_{ij} , and interatomic Coulomb integrals K_{ij} , are determined for each value of α and R (see section 2 for the details).

For this reason, specially-designed GS correlation functions, not only signaling the Mott transition in the thermodynamic limit, but also showing fast convergence (with $1/N \rightarrow 0$) for finite systems close to the metal–insulator boundary, may constitute a valuable complement of the existing numerical techniques.

In attempt to propose such correlation functions, one need to point out the relevance of quantum fluctuations between electronic doubly-occupied sites and unoccupied sites and between singly occupied sites with spin up and spin down in lattice models, as suggested before by numerous authors [15–19]. The concept quantum entanglement [20, 21], together with entanglement measures such as the concurrence [22], was adopted to quantify the above-mentioned fluctuations in various systems [23–25, 26–41], including basic spin models [23–25, 42], fermionic systems [26–31], or systems with spin and orbital degrees of freedom [32–35]. For an open fermionic system (namely: a correlated quantum dot attached to the leads) we found that the concurrence, defined separately for charge and spin degrees of freedom, allowed one to distinguish between different quantum transport regimes of the system [36]. Analogs of this observation were also reported for double [37, 38] and triple quantum dots [39]. For closed systems, in particular for small molecules, Mottet *et al* [40] showed that the entanglement analysis provided a valuable insight into the chemical bond formation. Even noninteracting systems with complex Fermi surface topology were characterized via their entanglement spectra [41]. Also very recently, a generic variational approach to correlated quantum systems, in which the output numerical precision is steered by setting maximal allowed entanglement between a selected subsystem and the environment, was proposed [43].

Sacramento *et al* [44] used entanglement measures to complement the long-lasting discussion of decoupling of charge and spin degrees of freedom in 1D Hubbard model [45] and its relation to the charge–spin separation phenomenon in Luttinger liquids [46, 47]. In particular, it is pointed out in [44] that charge–charge fluctuations, when quantified by properly defined correlation functions, show substantially different asymptotic behavior than spin–spin fluctuations in both the metallic and the insulating phases.

Here we focus on linear chains containing up to $N = 20$ equally-spaced hydrogenic-like atoms, each one containing a single valence orbital (see figure 1). Although such chains are not directly observable due to the well-known Peierls instability, they have been intensively studied to benchmark different *ab initio* approaches to strongly-correlated systems [48]. In this paper, two distinct physical regimes are considered: at the half filling the system shows a crossover behavior, with the increasing interatomic distance R , from a *partly localized* quantum liquid to the Mott insulating phase [3, 49]. At the quarter filling, the Mott transition is reconstructed with $1/N \rightarrow 0$ [3]. (The above-mentioned findings are consistent with more recent results of QMC simulations for Hubbard chains with long-range interactions [50].) It is worth to mention that the two regimes are also significantly different from a more fundamental point of view: in the strong-coupling (i.e., large R) limit the charge fluctuations are suppressed and the half-filled chain can be effectively described as 1D Heisenberg antiferromagnet, for which long-range order is absent due to the Mermin–Wagner theorem [51]. For the quarter-filling similar reasoning cannot be applied in the presence of long-range Coulomb interactions, and the charge-density wave phase is predicted to appear [3, 52–54]. In other words, we consider the two complementary model cases allowing one to test entanglement-based phase-transition indicators. We further discuss the concurrence [22], defined separately for charge and spin degrees of freedom, and employ it to recognize the decoupling of charge and spin degrees of freedom accompanying a finite-system version of the Mott transition.

The paper is organized as follows. In section 2 we present the system Hamiltonian and summarize the EDABI method. In section 3 the findings of [3], concerning the finite-size scaling of charge-energy gap, are revisited after taking larger systems under consideration. In section 4 we determine the local and pairwise entanglement, the latter for charge and spin degrees of freedom, and discuss their evolution with the interatomic distance and the system size. The conclusions are given in section 5.

2. The exact diagonalization—*ab initio* method (EDABI)

The EDABI method, together with its application to the system of figure 1, have been presented in several works [3–5, 49]. Here we briefly recall the main findings, to which we refer in the remaining parts of the paper.

2.1. The Hamiltonian for a linear chain

The analysis starts from the second-quantized Hamiltonian, which can be written in the form

$$\hat{\mathcal{H}}(\alpha, R) = \epsilon_a \sum_j \hat{n}_j + \sum_{i<j, \sigma} t_{ij} (\hat{c}_{i\sigma}^\dagger \hat{c}_{j\sigma} + \hat{c}_{j\sigma}^\dagger \hat{c}_{i\sigma}) + U \sum_i \hat{n}_{i\uparrow} \hat{n}_{i\downarrow} + \sum_{i<j} K_{ij} \hat{n}_i \hat{n}_j + V_{\text{ion-ion}}, \quad (1)$$

where ϵ_a is the atomic energy (same for all N sites upon applying periodic boundary conditions), t_{ij} is the hopping integral between i th and j th site (we further set $t_{ij} \equiv -t$ if i and j are nearest neighbors, otherwise $t_{ij} \approx 0$), U is the intrasite Coulomb repulsion, K_{ij} is the intersite Coulomb repulsion, and $V_{\text{ion-ion}} = \sum_{i<j} e^2/R_{ij}$ (with the distance $R_{ij} \equiv R \min(|i-j|, N-|i-j|)$) expresses the repulsion of infinite-mass ions.

The single-particle and interaction parameters of the Hamiltonian $\hat{\mathcal{H}}(\alpha, R)$ (1), also marked in figure 1, can be defined as follows

$$\langle w_i | T | w_j \rangle = \int d^3r w_i^*(\mathbf{r}) T(\mathbf{r}) w_j(\mathbf{r}) \equiv \epsilon_a \delta_{ij} + t_{ij} (1 - \delta_{ij}), \quad (2)$$

$$\langle w_i w_j | V | w_i w_j \rangle = \int d^3r d^3r' |w(\mathbf{r})|^2 V(\mathbf{r} - \mathbf{r}') |w(\mathbf{r}')|^2 \equiv U \delta_{ij} + K_{ij} (1 - \delta_{ij}), \quad (3)$$

where T is the single particle Hamiltonian describing an electron in the medium of periodically arranged ions, and V is the Coulomb repulsive interaction of two electrons. The Wannier functions are defined via atomic (Slater-type) functions, namely

$$w_i(\mathbf{r}) = \sum_j \beta_{ij} \psi_j(\mathbf{r}), \quad (4)$$

where the Slater $1s$ function $\psi_i(\mathbf{r}) = (\alpha^3/\pi)^{1/2} \exp(-\alpha|\mathbf{r} - \mathbf{R}_i|)$, with α being the inverse orbital size, here taken as variational parameter, and \mathbf{R}_i being the position of i th ion. The coefficients β_{ij} in equation (4) can be uniquely defined by imposing that (i) $\langle w_i | w_k \rangle = \delta_{ik}$ and that (ii) $\langle w_i | \psi_i \rangle$ is maximal [3, 55].

The range of Coulomb interactions in the Hamiltonian $\hat{\mathcal{H}}(\alpha, R)$ (1), quantified by parameters $K_{ij} \approx e^2/R_{ij}$ for $R_{ij} \gg R$, is *a priori* limited only by the chain length $L \equiv NR$. Previous studies on linear chains, both *ab initio* ones [12, 48] and these starting from second-quantized model Hamiltonians [50, 52], usually have imposed some form of charge screening reducing the range of such interactions (leaving the on-site Coulomb repulsion only in the extreme case [53]). This can be partly justified by possible influence of the environment in condensed-matter realizations such as quantum wires [54] or self-organized chains [56]. A slightly different situation occurs for cold atom systems, where long-range dipole–dipole interactions may be relevant [57]. Apart from these experiment-related premises, long-range interactions usually lead to a noticeable slowdown of the convergence for numerical methods such as DMRG or QMC [58, 59]. This is not the case for the EDABI method, as the determination of parameters K_{ij} corresponds to a relatively small portion of the overall computation time [60]², and the convergence of subsequent diagonalization in the Fock space (see the next subsection) is unaffected by the fact whether or not long-range interactions are included. Also, as charge screening becomes systematically less effective when the system dimensionality is reduced [61], one can expect it to be insignificant in a hypothetical realization of chains containing $N \leq 20$ atoms.

2.2. Single-particle basis optimization

Next, each Slater function is approximated as follows

$$\psi_i(\mathbf{r}) \approx \alpha^{3/2} \sum_{q=1}^p B_q \left(\frac{2\Gamma_q^2}{\pi} \right)^{3/4} e^{-\alpha^2 \Gamma_q^2 |\mathbf{r} - \mathbf{R}_i|^2}, \quad (5)$$

where p is the number of Gaussian functions truncating ψ_j , and $\{B_q, \Gamma_q\}$, $q = 1, \dots, p$, are adjustable parameters chosen to minimize the atomic energy for $\alpha = 1$ and a given value of p . Here we set $p = 3$, for which the deviation from the exact energy for $1s$ function is lower than 1%³. Subsequently, the parameters ϵ_a , t_{ij} , U , and K_{ij} are calculated from equations (2) and (3) as functions of α and R . The Hamiltonian $\hat{\mathcal{H}}(\alpha, R)$ (1) is diagonalized numerically in the Fock space, using the Lanczos algorithm, and the orbital size is optimized to find $\alpha = \alpha_{\min}$ corresponding to the minimal GS energy $E_G(N)$ for each R . Defining the effective atomic energy as

² The situation may become substantially different in the absence of translational invariance, see [60].

³ See appendix A in [55].

Table 1. Microscopic parameters (specified in eV—unless stated otherwise) of the Hamiltonian $\hat{\mathcal{H}}(\alpha, R)$ (1) with $\alpha = \alpha_{\min}$ minimizing the ground-state (GS) energy E_G . The Bohr radius is $a_0 = 0.529 \text{ \AA}$. The effective atomic level ϵ_a^{eff} is defined by equation (6); the remaining symbols are $t \equiv -t_{ij}$ for $j = i \pm 1 \pmod{N}$, $K_m \equiv K_{|i-j|}$ (with $m = 1, 2, 3$), and the correlated hopping integral $V \equiv \langle w_i w_j | V | w_i w_{i \pm 1} \rangle$, quantifying the largest neglected term in $\hat{\mathcal{H}}(\alpha, R)$. The numerical extrapolation with $1/N \rightarrow 0$ is performed for all parameters.

R/a_0	$\alpha_{\min} a_0$	ϵ_a^{eff}	t	U	K_1	K_2	K_3	V	E_G/N
1.5	1.363	1.36	11.31	27.95	15.85	9.08	6.08	−0.597	−10.19
2.0	1.220	−7.48	6.02	23.58	12.40	6.82	4.54	−0.324	−12.65
2.5	1.122	10.85	3.60	20.83	10.20	5.46	3.63	−0.203	−13.32
3.0	1.062	12.27	2.32	19.14	8.69	4.54	3.02	−0.150	−13.48
3.5	1.031	12.90	1.57	18.16	7.58	3.89	2.60	−0.128	−13.50
4.0	1.013	13.20	1.08	17.57	6.71	3.40	2.27	−0.119	−13.50
5.0	1.004	13.43	0.51	17.12	5.43	2.72	1.81	−0.096	−13.50
6.0	1.001	13.48	0.23	16.99	4.53	2.27	1.51	−0.058	−13.50
7.0	1.000	13.49	0.10	16.97	3.89	1.99	1.29	−0.027	−13.50

Table 2. Boundary conditions BC (with +/− marking the periodic/antiperiodic BC) and dimension of the largest subblock of the Hilbert space (with the total z th component of spin $S_z = 0$) for chains studied in the paper at the quarter filling (i.e., $N_{\text{el}} = N/2$). The last column specifies the values of the interatomic distance R_* at which the spin concurrence vanishes, with the interpolation errorbars for the last digit given in parenthesis. (See section 4 for details.)

N	N_{el}	BC	$\dim H(S_z^{\text{tot}} = 0)$	R_*/a_0
8	4	−	784	6.53(3)
12	6	+	48 400	5.22(2)
16	8	−	3 312 400	4.38(1)
20	10	+	240 374 016	4.51(1)

$$\epsilon_a^{\text{eff}} = \epsilon_a + \frac{1}{N} \left(\sum_{i < j} K_{ij} + V_{\text{ion-ion}} \right), \quad (6)$$

one finds that α_{\min} and other parameters converges rapidly with N . This observation allows us to speed up computations by using the values obtained for smaller systems ($N \geq 10$) to perform extrapolation with $1/N \rightarrow 0$. (The results are listed in table 1.)

3. Finite-size scaling for the charge-energy gap

A standard numerical approach [14, 50], allowing one to determine whether a correlated system described by the Hamiltonian such as given by equation (1) is metallic or insulating in the GS, involves calculating the charge-energy gap according to

$$\Delta E_C^{N_{\text{el}}}(N) = E_G^{N_{\text{el}}+1}(N) + E_G^{N_{\text{el}}-1}(N) - 2E_G^{N_{\text{el}}}(N), \quad (7)$$

where N_{el} is the number of electrons. Next, the limit of $1/N \rightarrow 0$ (with $N_{\text{el}}/N = \text{const}$) is to be taken numerically. The limiting value of $\Delta E_C \rightarrow 0$ indicates the metallic phase, whereas a nonzero value indicates the insulating phase⁴. In the numerical examples presented here and in section 4 we consider two different physical situations: the *half filling* $N_{\text{el}} = N$, with $N \leq 16$, and the *quarter filling* $N_{\text{el}} = N/2$, with $N \leq 20$; we further restrict ourselves to even values of N and N_{el} . Due to the total spin conservation it is sufficient, for each pair (N, N_{el}) , to look for the ground-state energy $E_G^{N_{\text{el}}}(N)$ in equation (7) in the subspace characterized by the total z th component of spin $S_z = 0$. Analogously, the values $E_G^{N_{\text{el}} \pm 1}(N)$ can be found by choosing $S_z = 1/2$. In particular, the largest considered subspace dimension corresponds to $N = 20$, $N_{\text{el}} + 1 = 11$, and is equal to 600 935 040. Moreover, we impose the periodic ($t_{i,j+N} = t_{ij}$) or antiperiodic ($t_{i,j+N} = -t_{ij}$) boundary conditions to minimize $E_G^{N_{\text{el}}}(N)$ for $N_{\text{el}} = 4k + 2$ or $N_{\text{el}} = 4k$, respectively, with k -integer (see table 2).

⁴ Strictly speaking, finding out whether the insulating phase is of the Mott type also requires calculation of the so-called spin gap, $\Delta E_S = E_G^{S_z=1} - E_G^{S_z=0}$ (where $E_G^{S_z}$ denotes the lowest eigenenergy in the subspace with a total z th component of spin S_z); $\Delta E_C > 0$ accompanied by $\Delta E_S \rightarrow 0$ for $1/N \rightarrow 0$ indicates the Mott phase. Although the answer may not be obvious in a more general situation (see [13], footnote 1), a lack of long-range spin order in 1D systems manifests itself by a fast decay of ΔE_S with N for atomic chains described by the Hamiltonian $\hat{\mathcal{H}}(\alpha, R)$ (1) for all values of R . The numerical demonstrations are provided in [3, 55].

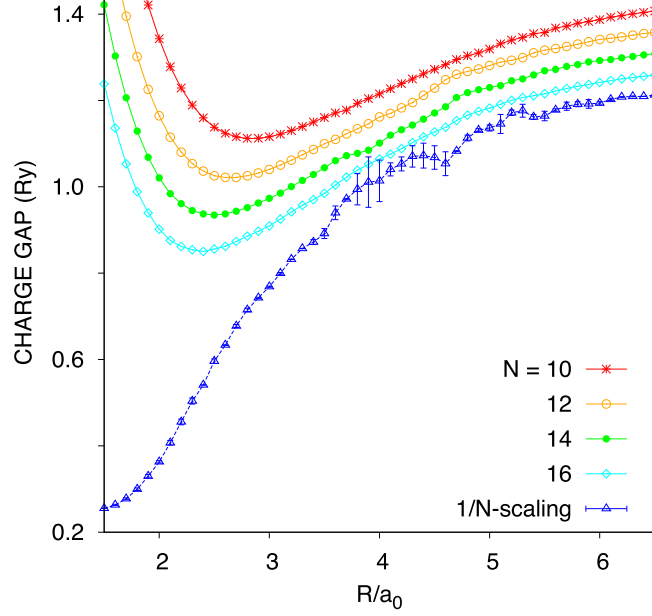


Figure 2. Charge-energy gap as a function of the interatomic distance R/a_0 (with the Bohr radius $a_0 = 0.529 \text{ \AA}$) for chains of $N = 10$ – 16 atoms at the *half filling* ($N_{\text{el}} = N$). Datapoints were shifted vertically by 0.05 Ry for $N = 16$ (diamonds), 0.10 Ry for $N = 14$ (solid circles), 0.15 Ry for $N = 12$ (open circles), or 0.20 Ry for $N = 10$ (stars). The results of the finite-size scaling with $1/N \rightarrow 0$, obtained via the Richardson extrapolation of the second order [62], are also shown (triangles). Lines are guides for the eye only.

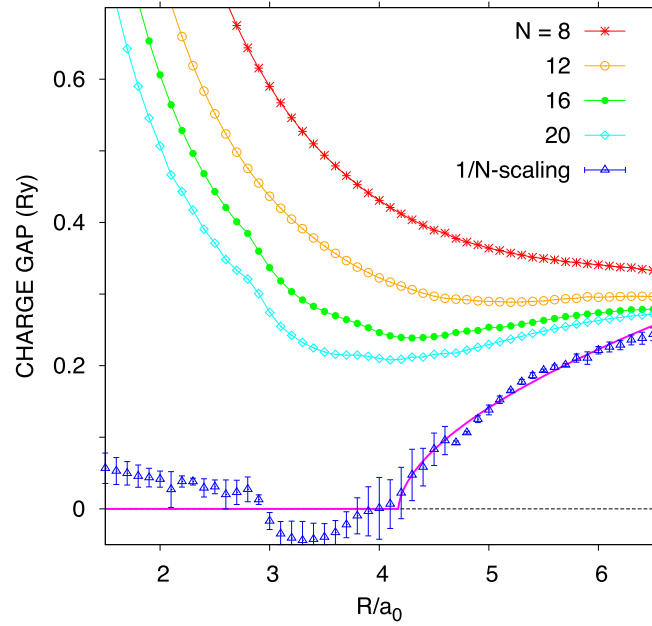


Figure 3. Same as figure 2 but for chains of $N = 8$ – 20 atoms at the *quarter filling* ($N_{\text{el}} = N/2$). No artificial dashshifts were applied this time. Horizontal dashed line marks $\Delta E_C = 0$, solid purple line represents the best-fitted function given by equations (8) and (9), indicating the Mott metal–insulator transition in the $1/N \rightarrow 0$ limit, occurring for $R = R_c \approx 4.2 a_0$.

The numerical results, corresponding to the Hamiltonian $\hat{\mathcal{H}}(\alpha, R)$ (1) with the microscopic parameters listed in table 1, are presented in figures 2 and 3. We notice that the datasets for $N \leq 14$ at the half filling as well as for $N \leq 16$ at the quarter filling were presented in [3], where we also used the Richardson extrapolation of the second order [62] to perform finite-size scaling with $1/N \rightarrow 0$ for each value of R . After adding the new datasets for $N = 16$, $N_{\text{el}} = N$ and $N = 20$, $N_{\text{el}} = N/2$ (both depicted with open diamonds) the earlier conclusions regarding the system GS are further supported: namely, the extrapolation with $1/N \rightarrow 0$ (open triangles) at $N_{\text{el}} = N$ leads to $\Delta E_C > 0$ for any accessible value of R/a_0 indicating the insulating phase (see figure 2). At

$N_{\text{el}} = N/2$, the finite-size scaling results can be rationalized with the empirical function

$$\Delta E_C^{N/2}(1/N \rightarrow 0) \approx \begin{cases} 0 & \text{if } R < R_c, \\ \Delta_0[(R - R_c)/a_0]^\gamma & \text{if } R \geq R_c, \end{cases} \quad (8)$$

with the best-fitted parameters (numbers in parentheses are standard deviations for the last digit)

$$R_c = 4.18(2)a_0, \quad \Delta_0 = 0.158(3)\text{Ry}, \quad \gamma = 0.57(3), \quad (9)$$

depicted with solid purple line in figure 3. The gap opening at $R = R_c$ indicates the Mott transition.

For a sake of conciseness, our discussion of finite-size scaling estimates of the Mott transition is limited to the charge-energy gap. A more detailed analysis, presented in [3, 49, 55] and involving calculations of the electron momentum distribution, the Drude weight, as well as the so-called modern theory of polarization [63], justify the transition appearance in the $N_{\text{el}} = N/2$ case, which coincides with the results for related parametrized model studies [50, 52, 53, 57]. In the $N_{\text{el}} = N$ case, the situation is of a slightly more complex nature: apart from a nonzero gap for any R , following from the finite-size scaling, several GS and dynamical characteristics (in particular—the Drude weight, see [3]) exhibit, for any finite N , a crossover behavior between a partly localized quantum liquid, appearing for small R , and a fully-reconstructed Mott insulator, typically appearing for $R/a_0 \gtrsim 4$. These findings coincide with more recent variational Monte-Carlo studies of hydrogenic chains (see [12]), and can be attributed to the increasing (with growing R) role of electron correlations in either the exact or variational GS wavefunction.

It is worth to mention here that some surprisingly efficient variational methods, such as presented in [12], become significantly less efficient when treating open-shell configurations in attempt to calculate ΔE_C from equation (7), or generally when utilized away from the half filling ($N_{\text{el}} \neq N$). Also for this reason, GS correlation functions signaling a finite-system version of the Mott transition for N small enough to be treated with some more flexible numerical techniques, are desired.

4. Reduced density matrix and quantum entanglement

In this section we derive explicit representations of the reduced density operator $\hat{\rho}_A = \text{Tr}_B |\Psi\rangle\langle\Psi|$ (where Tr_B stands for tracing over all degrees of freedom except from those characterizing a selected subsystem A) relevant when discussing the local entanglement, the pairwise entanglement for charge degrees of freedom, and the pairwise entanglement for spin degrees of freedom. The derivations remain valid for a generic spin-1/2 fermionic system at any pure state $|\Psi\rangle$, which can be represented assuming four basis states for each site j , namely:

$$\{|n_{j\uparrow}n_{j\downarrow}\rangle\} \equiv \{|0\rangle_j, |\uparrow\uparrow\rangle_j, |\downarrow\downarrow\rangle_j, |\uparrow\downarrow\rangle_j\}; \quad (10)$$

although the numerical examples, considered in search for entanglement-based estimates of the Mott transition, all correspond to the GS of a linear chain described by the Hamiltonian $\hat{\mathcal{H}}(\alpha, R)$ (1) with the microscopic parameters taken from table 1.

4.1. General considerations

Let us consider a general example at first: the quantum system, which can be divided into two distinct subsystems A and B . A pure state $|\Psi\rangle$ can be represented as follows

$$|\Psi\rangle = \sum_{\alpha\beta} \Psi_{\alpha\beta} |\alpha\rangle \otimes |\beta\rangle, \quad (11)$$

where $\Psi_{\alpha\beta}$ denotes a complex probability amplitude corresponding to a basis state of the full system $|\alpha\rangle \otimes |\beta\rangle$, while $\{|\alpha\rangle\}$ and $\{|\beta\rangle\}$ are complete basis sets for the subsystems A and B (respectively). The reduced density operator $\hat{\rho}_A$ is defined as:

$$\begin{aligned} \hat{\rho}_A &= \text{Tr}_B |\Psi\rangle\langle\Psi| \equiv \sum_{\beta} \langle\beta|\Psi\rangle\langle\Psi|\beta\rangle \\ &= \sum_{\beta, \alpha, \alpha'} \Psi_{\alpha\beta} \Psi_{\alpha'\beta}^* |\alpha\rangle\langle\alpha'|, \end{aligned} \quad (12)$$

where the last equality follows from equation (11) and $\Psi_{\alpha'\beta}^*$ denotes the complex conjugate of $\Psi_{\alpha\beta}$. Subsequently, the matrix elements of $\hat{\rho}_A$ are given by

$$\rho_{\alpha, \alpha'} \equiv \langle\alpha|\hat{\rho}_A|\alpha'\rangle = \sum_{\beta} \Psi_{\alpha\beta} \Psi_{\alpha'\beta}^*. \quad (13)$$

We define now projection operators P_α and P_β , associated with the basis states $|\alpha\rangle$ and $|\beta\rangle$, via

$$P_\alpha|\alpha'\rangle = \delta_{\alpha\alpha'}|\alpha\rangle, \quad P_\beta|\beta'\rangle = \delta_{\beta\beta'}|\beta\rangle. \quad (14)$$

Useful properties, directly following from equation (14) are

$$P_\alpha^2 = P_\alpha, \quad P_\beta^2 = P_\beta, \quad (15)$$

$$\sum_\alpha P_\alpha = \sum_\beta P_\beta = 1, \quad (16)$$

where equation (16) also employs the completeness of the basis sets $\{|\alpha\rangle\}$ and $\{|\beta\rangle\}$. Next, we define the transfer operator

$$T_{\alpha\alpha'}|\alpha'\rangle = |\alpha\rangle, \quad \langle\alpha'|T_{\alpha\alpha'}^\dagger = \langle\alpha|, \quad (17)$$

which is unitary, i.e.

$$T_{\alpha\alpha'}^\dagger = (T_{\alpha\alpha'})^{-1} \equiv T_{\alpha'\alpha}. \quad (18)$$

Explicit forms of P_α , P_β , and $T_{\alpha\alpha'}$, corresponding to the particular splittings of the system into A and B subsystems, are to be specified later in terms of the operators $\{\hat{c}_{i\sigma}, \hat{c}_{i\sigma}^\dagger\}$ for lattice spin-1/2 fermions. Here we notice that as the indices (α, α') refer the subsystem A , whereas the index β refers to the subsystem B , we have

$$[P_\alpha, P_\beta] = 0, \quad [P_\beta, T_{\alpha\alpha'}] = 0, \quad (19)$$

for all (α, α') and β .

With the help of operators P_α and P_β (14) one can write down, for $|\Psi\rangle$ represented according to equation (11),

$$P_\alpha P_\beta |\Psi\rangle = \Psi_{\alpha\beta} |\alpha\rangle \otimes |\beta\rangle, \quad (20)$$

$$\langle\Psi|P_{\alpha'}P_\beta = \langle\alpha'| \otimes \langle\beta| \Psi_{\alpha'\beta}^*. \quad (21)$$

In turn, the reduced density matrix, as given by the rightmost equality in equation (13), can be rewritten as

$$\begin{aligned} \rho_{\alpha\alpha'} &= \sum_\beta \langle\Psi|P_{\alpha'}P_\beta T_{\alpha'\alpha} P_\alpha P_\beta |\Psi\rangle \\ &= \langle\Psi|P_{\alpha'} T_{\alpha'\alpha} P_\alpha |\Psi\rangle, \end{aligned} \quad (22)$$

with the last equality following from equations (15), (16), and (19). Finally, using equation (18), we find

$$(\rho_{\alpha\alpha'})^* = \langle\Psi|P_\alpha T_{\alpha\alpha'} P_{\alpha'} |\Psi\rangle. \quad (23)$$

Remarkably, the reduced density matrix elements in equation (23) are expressed by pure-state expectation values (correlation functions) of the operators acting only on the subsystem A . This feature is further explored in the remaining parts of this section.

4.2. Entanglement entropy

The local entanglement [27] exhibits quantum correlations between the local state of a selected j th site (subsystem A) and the rest of the system (B). As the basis set $\{|\alpha\rangle\}$ is simply given by equation (10), one can write down the corresponding projection operators

$$(P_\alpha) = [(1 - n_\uparrow)(1 - n_\downarrow), n_\uparrow(1 - n_\downarrow), (1 - n_\uparrow)n_\downarrow, n_\uparrow n_\downarrow]^T, \quad (24)$$

and the transfer operators

$$(T_{\alpha\alpha'}) = \begin{pmatrix} 1 & c_\uparrow & c_\downarrow & c_\downarrow c_\uparrow \\ c_\uparrow^\dagger & 1 & c_\uparrow^\dagger c_\downarrow & -c_\downarrow \\ c_\downarrow^\dagger & c_\downarrow^\dagger c_\uparrow & 1 & c_\uparrow \\ c_\uparrow^\dagger c_\downarrow^\dagger & -c_\downarrow^\dagger & c_\uparrow^\dagger & 1 \end{pmatrix}, \quad (25)$$

where we have omitted the site index j for brevity. For the system with the total spin and charge conservation, such as our linear chain (see equation (1)), we have

$$\begin{aligned} \langle c_\sigma \rangle &= \langle c_\sigma^\dagger \rangle = 0, \quad \langle c_\sigma c_{\bar{\sigma}} \rangle = \langle c_\sigma^\dagger c_{\bar{\sigma}}^\dagger \rangle = 0, \\ \text{and} \quad \langle c_\sigma^\dagger c_{\bar{\sigma}} \rangle &= \langle c_{\bar{\sigma}}^\dagger c_\sigma \rangle = 0, \end{aligned} \quad (26)$$

(with $\bar{\sigma}$ being the spin index opposite to σ) providing that the averaging takes place over an eigenstate $|\Psi\rangle$ of the system Hamiltonian (not necessarily the GS). Substituting the expressions for P_α (24) and $T_{\alpha\alpha'}$ (25) into equation (23) and taking equation (26) into account we get, after a straightforward algebra,

$$(\rho_{\alpha\alpha'}) = \text{diag}(u_+, w_1, w_2, u_-) \quad (27)$$

with

$$\begin{aligned} u_+ &= \langle (1 - n_{j\uparrow})(1 - n_{j\downarrow}) \rangle, & w_1 &= \langle n_{j\uparrow}(1 - n_{j\downarrow}) \rangle, \\ w_2 &= \langle (1 - n_{j\uparrow})n_{j\downarrow} \rangle, & u_- &= \langle n_{j\uparrow}n_{j\downarrow} \rangle. \end{aligned} \quad (28)$$

Equation (27) corresponds to the reduced density operator of the well-known form

$$\hat{\rho}_A = \sum_{\alpha\alpha'} \rho_{\alpha\alpha'} |\alpha\rangle \langle \alpha'| = u_+ |0\rangle \langle 0| + w_1 |\uparrow\rangle \langle \uparrow| + w_2 |\downarrow\rangle \langle \downarrow| + u_- |\uparrow\downarrow\rangle \langle \uparrow\downarrow|, \quad (29)$$

where we have used the basis given by equation (10).

A quantitative measure of the entanglement between the state of j th site and that of the remaining $N - 1$ sites is given by the von Neumann entropy

$$E_v = -u_+ \log_2 u_+ - w_1 \log_2 w_1 - w_2 \log_2 w_2 - u_- \log_2 u_-. \quad (30)$$

If the translational invariance of the system is imposed, one can define the particle density n and the average number of double occupancies d , following

$$\langle n_{j\uparrow} \rangle = \langle n_{j\downarrow} \rangle = \frac{N_{\text{el}}}{2N} \equiv \frac{n}{2}, \quad \langle n_{j\uparrow} n_{j\downarrow} \rangle \equiv d, \quad (31)$$

where we have further assumed that the averaging takes place over an eigenstate characterized by the total z th component of spin $S_z = 0$. Subsequently, equation (28) can be rewritten as

$$u_+ = 1 - n + d, \quad w_1 = w_2 = \frac{n}{2} - d, \quad u_- = d. \quad (32)$$

In particular, for the GS of the Hamiltonian $\hat{\mathcal{H}}(\alpha, R)$ (1), for which the effective interaction between electrons can roughly be estimated by $\sim U - K_1$ and is always repulsive, one can show that

$$\frac{|n - 1| + n - 1}{2} \leq d \leq \frac{n^2}{4} \quad \text{for} \quad 0 \leq n \leq 2, \quad (33)$$

where the lower bound for d corresponds to the so-called *strong-correlations limit* approached for $R \gg a_0$ (as the bandwidth $W \equiv 4t \ll U - K_1$, see table 1), whereas the upper bound for d corresponds to the *free-electrons limit* approached for $R \lesssim 2a_0$ ($W \gg U - K_1$). As the charge fluctuations are given by $\text{Var}\{n_j\} = \langle n_j^2 \rangle - \langle n_j \rangle^2 \equiv n - n^2 + 2d$, the above-mentioned limits coincide (respectively) with the minimal and the maximal fluctuations for a given n . Moreover, the bounds for d in equation (33) can be mapped, via equation (32), onto

$$E_v^{\text{corr}}(n) \leq E_v \leq E_v^{\text{free}}(n), \quad (34)$$

with

$$E_v^{\text{corr}}(n) = -|1 - n| \log_2 |1 - n| - (1 - |1 - n|) \log_2 \left(\frac{1 - |1 - n|}{2} \right) \quad (35)$$

for the strong-correlations limit, and

$$E_v^{\text{free}}(n) = -n \log_2 \frac{n}{2} - (2 - n) \log_2 \left(1 - \frac{n}{2} \right) \quad (36)$$

for the free-electrons limit. For instance, equations (34)–(36) lead to

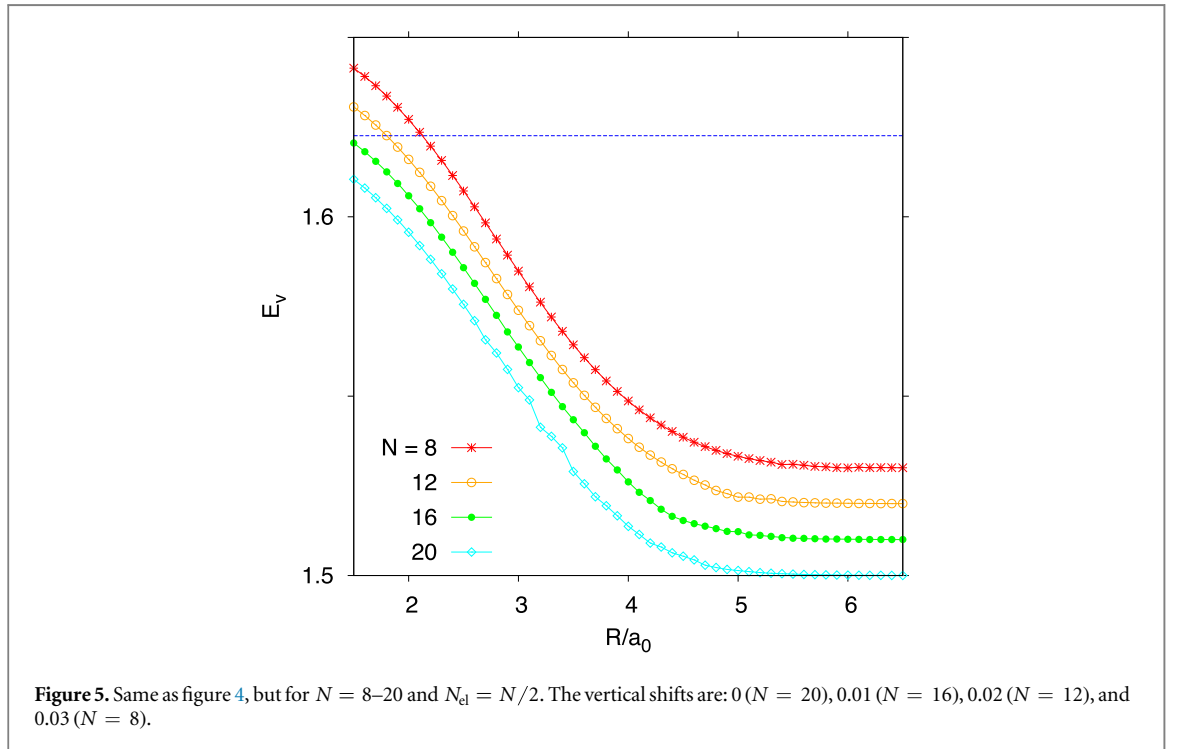
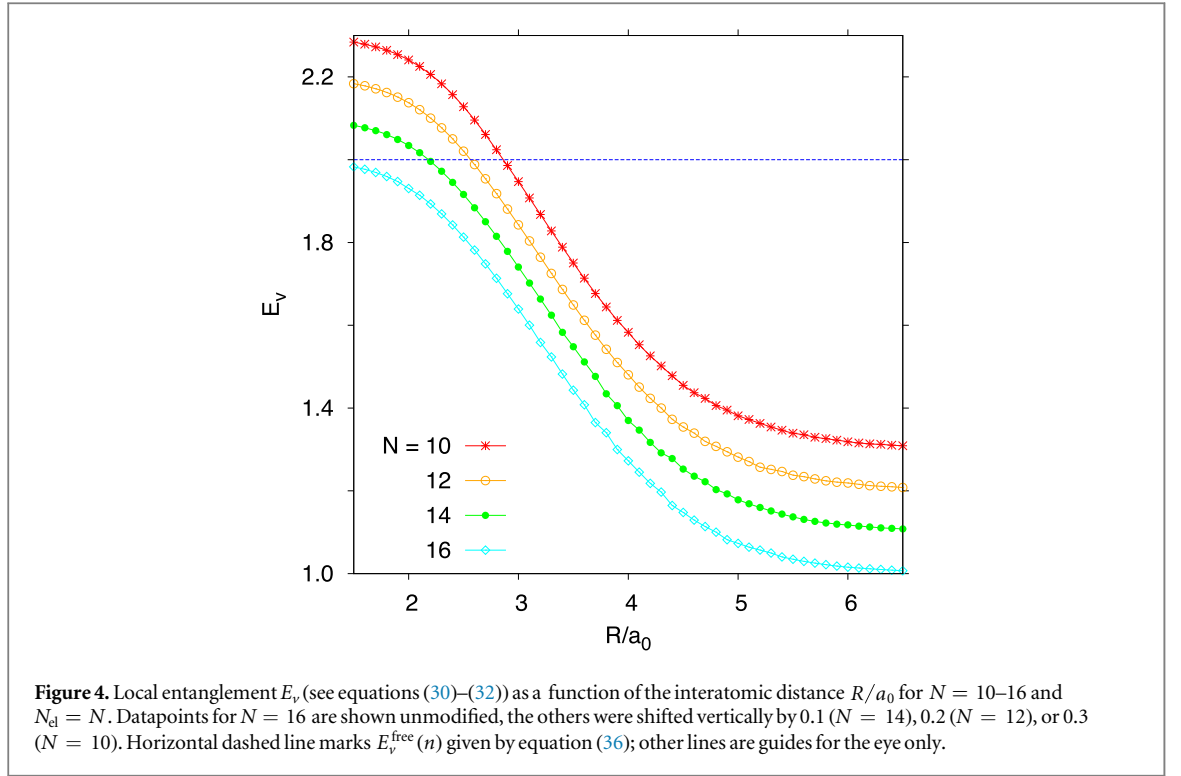
$$1 \leq E_v \leq 2 \quad \text{for} \quad N_{\text{el}} = N, \quad (37)$$

and

$$\frac{3}{2} \leq E_v \leq 4 - \frac{3}{2} \log_2 3 \approx 1.623 \quad \text{for} \quad N_{\text{el}} = \frac{N}{2}. \quad (38)$$

Remarkably, the strong-correlations limit corresponds to the minimal E_v , whereas the free-electrons limit corresponds to the maximal E_v (for any $0 \leq n \leq 2$). This is because when the free-electrons limit is approached, ground-state wavefunction can be truncated by a single Slater determinant composed of fully delocalized single-particle functions (Bloch functions), resulting in the maximal entanglement between j th site and the remaining $N - 1$ sites [12, 36]. Repulsive interactions between electrons lead to the correlation-induced suppression of $\text{Var}\{n_j\}$, and to the decreasing E_v with growing the interaction-to-bandwidth ratio.

General findings, presented briefly in the above, are now illustrated with the numerical examples for $N_{\text{el}} = N$ and $N_{\text{el}} = N/2$ (see figures 4 and 5). In both cases, the values of E_v are close to the upper bounds given by equations (37) and (38) for the smallest considered value of $R/a_0 = 1.5$, and systematically decrease with growing R , gradually approaching the lower bounds in equations (37) and (38). Also, a remarkably fast convergence of E_v with growing N is observed for any R , making it necessary to apply vertical shifts to the datasets



in figures 4 and 5. We further notice that $E_v \approx 3/2$ starting from $R \gtrsim 5 a_0$ for $N_{el} = N/2$, whereas for $N_{el} = N$ we still have $E_v > 1$ in this range. However, the smooth evolution of E_v with R is observed for both $N_{el} = N$ and $N_{el} = N/2$, making it difficult to consider the local entanglement as an estimate of the Mott transition. Pairwise entanglement is discussed next as the other candidate.

4.3. The fermionic concurrence

We consider now the subsystem A consists of two spatially-separate quantum bits (*qubits*), one of which is associated with i th lattice site and the other with j th site. Each individual qubit can be realized employing charge or spin degrees of freedom.

For instance, if *charge qubits* are under consideration, one can choose the basis set for A in a fixed-spin sector $\sigma = \uparrow$, namely

$$\{|\alpha\rangle\}^c = \{ |0\rangle_i \otimes |0\rangle_j, |0\rangle_i \otimes |\uparrow\rangle_j, |\uparrow\rangle_i \otimes |0\rangle_j, |\uparrow\rangle_i \otimes |\uparrow\rangle_j \}, \quad (39)$$

whereas for *spin qubits* we have

$$\{|\alpha\rangle\}^s = \{ |\uparrow\rangle_i \otimes |\uparrow\rangle_j, |\uparrow\rangle_i \otimes |\downarrow\rangle_j, |\downarrow\rangle_i \otimes |\uparrow\rangle_j, |\downarrow\rangle_i \otimes |\downarrow\rangle_j \}. \quad (40)$$

The corresponding projection operators are

$$(P_\alpha^c) = [(1 - n_{i\uparrow})(1 - n_{j\uparrow}), (1 - n_{i\uparrow})n_{j\uparrow}, n_{i\uparrow}(1 - n_{j\uparrow}), n_{i\uparrow}n_{j\uparrow}]^T, \quad (41)$$

and

$$(P_\alpha^s) = [n_{i\uparrow}(1 - n_{i\downarrow})n_{j\uparrow}(1 - n_{j\downarrow}), n_{i\uparrow}(1 - n_{i\downarrow})(1 - n_{j\uparrow})n_{j\downarrow}, \\ (1 - n_{i\uparrow})n_{i\downarrow}n_{j\uparrow}(1 - n_{j\downarrow}), (1 - n_{i\uparrow})n_{i\downarrow}(1 - n_{j\uparrow})n_{j\downarrow}]^T, \quad (42)$$

with the upper indices (c, s) referring to charge and spin qubits (respectively). Subsequently, the transfer operators are given by

$$(T_{\alpha\alpha'}^c) = \begin{pmatrix} 1 & c_{j\uparrow} & c_{i\uparrow} & c_{j\uparrow}c_{i\uparrow} \\ c_{j\uparrow}^\dagger & 1 & c_{j\uparrow}^\dagger c_{i\uparrow} & c_{i\uparrow} \\ c_{i\uparrow}^\dagger & c_{i\uparrow}^\dagger c_{j\uparrow} & 1 & -c_{j\uparrow} \\ c_{i\uparrow}^\dagger c_{j\uparrow}^\dagger & c_{i\uparrow}^\dagger & -c_{j\uparrow}^\dagger & 1 \end{pmatrix}, \quad (43)$$

and

$$(T_{\alpha\alpha'}^s) = \begin{pmatrix} 1 & S_j^+ & S_i^+ & S_j^+ S_i^+ \\ S_j^- & 1 & S_j^- S_i^+ & S_i^+ \\ S_i^- & S_i^- S_j^+ & 1 & S_j^+ \\ S_i^- S_j^- & S_i^- & S_j^- & 1 \end{pmatrix}, \quad (44)$$

with the spin operators $S_i^+ = c_{i\uparrow}^\dagger c_{i\downarrow}$, $S_i^- = c_{i\downarrow}^\dagger c_{i\uparrow}$. Substituting the above expressions into equation (23) we get

$$(\rho_{\alpha\alpha'}^X) = \begin{pmatrix} u_+^X & 0 & 0 & 0 \\ 0 & w_1^X & z^X & 0 \\ 0 & (z^X)^* & w_2^X & 0 \\ 0 & 0 & 0 & u_-^X \end{pmatrix} \quad \text{for } X = c, s, \quad (45)$$

where the total spin and charge conservation is imposed. The nonzero matrix elements in equation (45) are given by

$$u_+^c = \langle (1 - n_{i\uparrow})(1 - n_{j\uparrow}) \rangle, \quad w_1^c = \langle n_{i\uparrow}(1 - n_{j\uparrow}) \rangle, \\ z^c = \langle c_{j\uparrow}^\dagger c_{i\uparrow} \rangle, \quad w_2^c = \langle (1 - n_{i\uparrow})n_{j\uparrow} \rangle, \quad u_-^c = \langle n_{i\uparrow}n_{j\uparrow} \rangle, \quad (46)$$

for charge qubits, or by

$$u_+^s = \langle n_{i\uparrow}(1 - n_{i\downarrow})n_{j\uparrow}(1 - n_{j\downarrow}) \rangle, \\ w_1^s = \langle n_{i\uparrow}(1 - n_{i\downarrow})(1 - n_{j\uparrow})n_{j\downarrow} \rangle, \\ z^s = \langle S_j^+ S_i^- \rangle = \langle c_{j\uparrow}^\dagger c_{j\downarrow} c_{i\downarrow}^\dagger c_{i\uparrow} \rangle, \\ w_2^s = \langle (1 - n_{i\uparrow})n_{i\downarrow}n_{j\uparrow}(1 - n_{j\downarrow}) \rangle, \\ u_-^s = \langle (1 - n_{i\uparrow})n_{i\downarrow}(1 - n_{j\uparrow})n_{j\downarrow} \rangle, \quad (47)$$

for spin qubits.

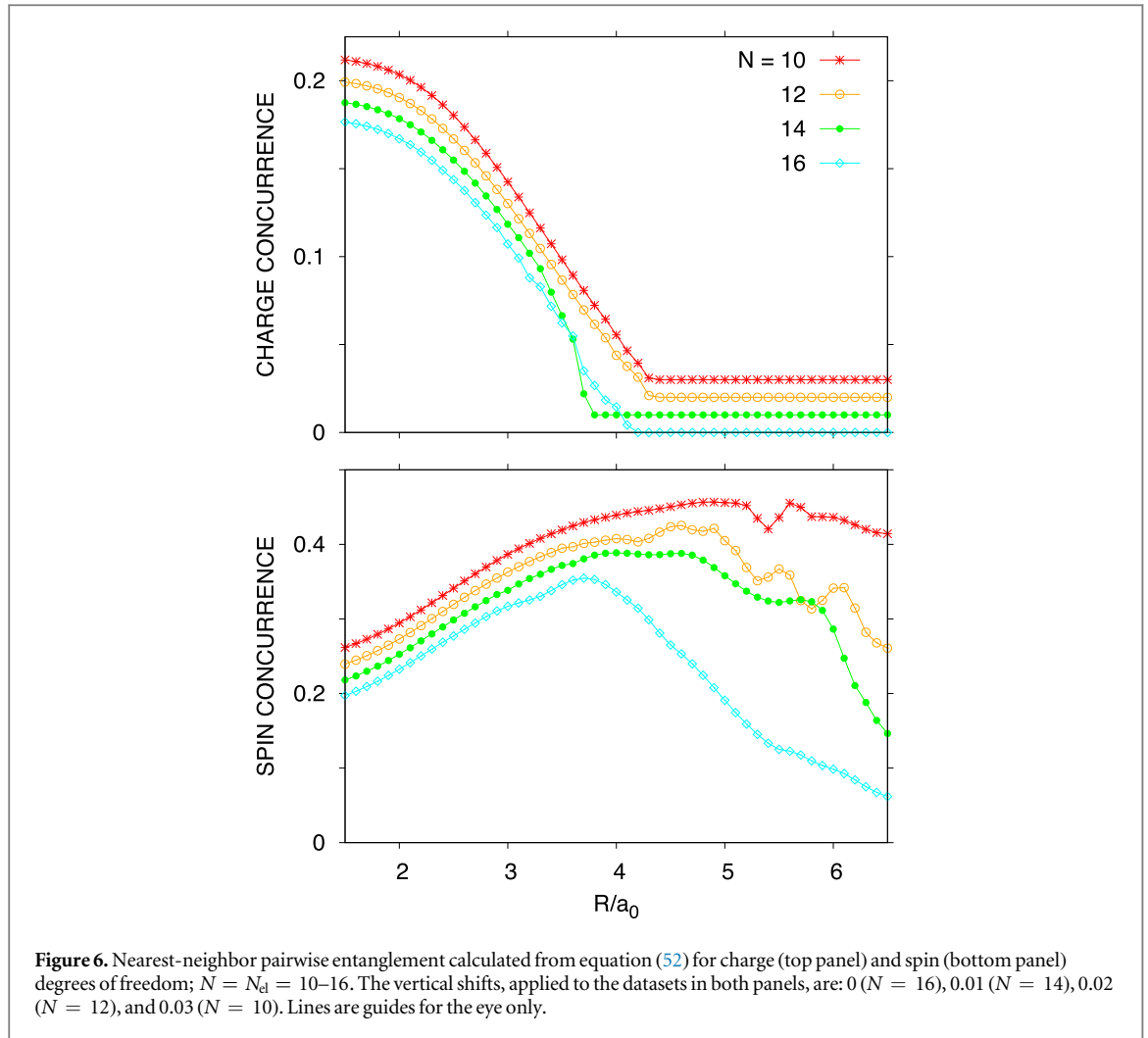
We use now the *concurrence* \mathcal{C} , as a quantitative measure of quantum entanglement in the two-qubit subsystem A . The closed-form expression was derived by Wootters [22] and reads

$$\mathcal{C} = \max \{0, \sqrt{\lambda_1} - \sqrt{\lambda_2} - \sqrt{\lambda_3} - \sqrt{\lambda_4}\}, \quad (48)$$

where $\lambda_1 \geq \lambda_2 \geq \lambda_3 \geq \lambda_4$ are eigenvalues of the matrix product

$$\rho \cdot (\sigma_i^y \otimes \sigma_j^y) \rho^* (\sigma_i^y \otimes \sigma_j^y) \quad (49)$$

with $\rho = (\rho_{\alpha\alpha'}^X)$ given by equations (45)–(47), and σ_i^y (σ_j^y) being the second Pauli matrix acting on the qubit associated with i th (j th) lattice site. It was also shown in [22] that the entanglement of formation for a pair of



qubits was uniquely determined by \mathcal{C} , namely

$$E_f = -\xi \log_2 \xi - (1 - \xi) \log_2 (1 - \xi), \quad (50)$$

where $\xi = (1 + \sqrt{1 - \mathcal{C}^2})/2$. In fact, \mathcal{C} can be interpreted as a distance between a given quantum state and the nearest separable state [64]. For these reasons, \mathcal{C} can be used to quantify the entanglement of two qubits instead of E_f and is hereinafter called *pairwise entanglement*.

The eigenvalues of the matrix defined by equation (49) can be written as

$$\begin{aligned} \tilde{\lambda}_1 &= \tilde{\lambda}_4 = u_+^X u_-^X, \\ \tilde{\lambda}_{2,3} &= (\sqrt{w_1^X w_2^X} \pm |z^X|)^2, \end{aligned} \quad (51)$$

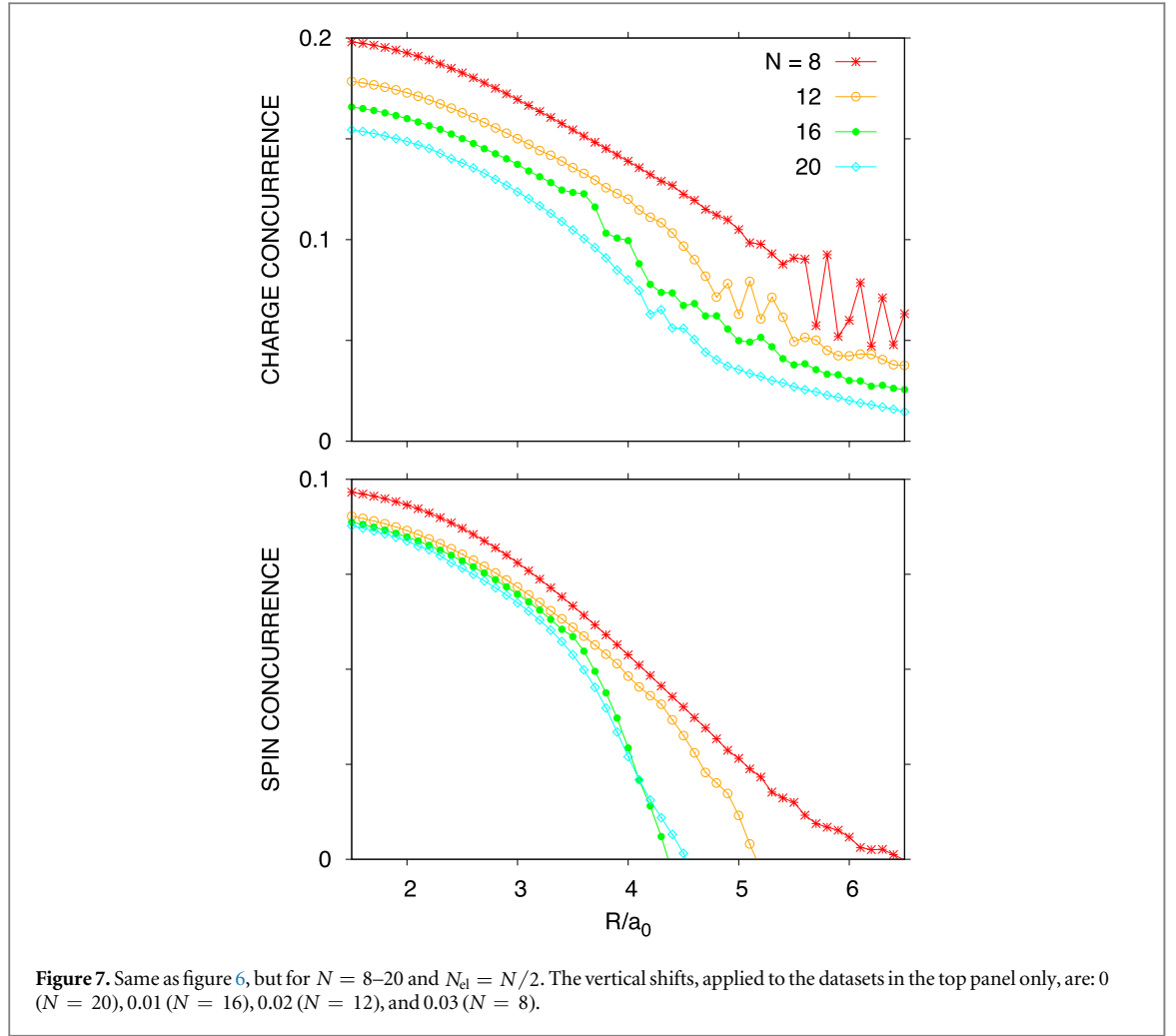
where $\tilde{\lambda}_1, \dots, \tilde{\lambda}_4$ are yet unsorted. After some straightforward steps, equation (48) leads to

$$\mathcal{C} = 2 \max \{0, |z^X| - \sqrt{u_+^X u_-^X}\}, \quad (52)$$

where the relevant correlation functions are given by equation (46) for $X = c$, or by equation (47) for $X = s$. The correlation functions w_1^X and w_2^X are absent in equation (52) as they contribute to $\sqrt{\lambda_1} - \sqrt{\lambda_2} - \sqrt{\lambda_3} - \sqrt{\lambda_4}$ if and only if $\sqrt{\lambda_1} - \sqrt{\lambda_2} - \sqrt{\lambda_3} - \sqrt{\lambda_4} < 0$.

Generalizations of \mathcal{C} for multifermionic states, appearing when larger subsystem A is under consideration, are also possible [65]. Such generalizations are, however, beyond the scope of this paper. We focus here on the pairwise entanglement, mainly because the form of equation (52) makes it possible to be determined with no significant computational costs once standard (spin or charge) correlation functions are calculated.

Our numerical results for the pairwise entanglement are presented in figures 6 and 7, constituting the central findings of this paper. The presentation is limited to the cases when sites i and j are the nearest neighbors in



a linear chain (i.e., $j = i \pm 1 \bmod N$), as we have found that $\mathcal{C} = 0$ for more distant neighbors⁵. Also, correlation functions in equation (52) are averaged over the reference site number i , to reduce the finite-precision effects.

For $N_{\text{el}} = N$, we have $\mathcal{C} = 0$ for the charge degrees of freedom (so-called *charge concurrence*) provided that $R/a_0 \gtrsim 4$ (see top panel in figure 6). In such a range, the separability of a quantum state in the position representation, appearing if a bipartite subsystem (A) is selected in a fixed-spin sector, justifies the above-used notion of a fully-reconstructed Mott insulator for a finite N (see section 3 and [3, 12]). For smaller R , stronger charge fluctuations manifest itself via nonzero charge concurrence, providing an insight into the nature of a partly-localized quantum liquid. Remarkably, spin concurrence (see bottom panel in figure 6) is positive for any considered N and R/a_0 , reaching the maximum in the crossover range of $4 \lesssim R/a_0 \lesssim 5$. For this reason, spin concurrence still can be considered as a prospective signature of the Mott transition.

For $N_{\text{el}} = N/2$ the evolution of the pairwise entanglement with R/a_0 (see figure 7) is significantly different than for the $N_{\text{el}} = N$ case. For each N , we have a nonzero charge concurrence for any considered R/a_0 (top panel in figure 7), whereas the spin concurrence (bottom panel) indicates a finite-system version of the Mott transition⁶. In brief, for spin degrees of freedom $\mathcal{C} = 0$ for $R > R_*(N)$, where the nodal value $R_*(N)$ corresponds to $|z^s| - \sqrt{u_+^s u_-^s} = 0$, and is determined numerically via least-squares fitting of a line to the actual datapoints for a given N (see the last column in table 2). For larger N , the values of $R_*(N)$ are close to $R_c \approx 4.2 a_0$, determined in section 3 via the finite-size scaling for ΔE_C .

Additionally, we observe that the nearest-neighbor pairwise entanglement may indicate the decoupling of charge and spin degrees of freedom in correlated systems. This happens for $R/a_0 \gtrsim 4$ in the $N_{\text{el}} = N$ case (as

⁵ This can be attributed to generic asymptotic behavior of the reduced density matrix (see equation (45)), for which $\rho_{\alpha\alpha'}^X \approx \left(\frac{1}{2}n\right)^2 \delta_{\alpha\alpha'}$ for $X = c$, or $\rho_{\alpha\alpha'}^X \approx \left(\frac{1}{2}n - d\right)^2 \delta_{\alpha\alpha'}$ for $X = s$, since the relevant operator-fluctuations in equations (46) and (47) become uncorrelated with growing the distance between sites i and j . Analogous features for spin models were discussed in [42].

⁶ We have intentionally limited the number of Lanczos iterations, starting (in any case) from a randomly-chosen vector in the Fock space, to relatively small value of $m = 30$. This allows us to visualize how GS correlation functions converges with the system size: notice that the oscillations of \mathcal{C} as a function of R , visible for $N = 8$ and 12 in figure 7, are strongly suppressed for larger N .

well as for $R > R_*(N)$ in the $N_{\text{el}} = N/2$ case), where nonzero spin (charge) concurrence is accompanied by vanishing charge (spin) concurrence. In the above-mentioned ranges, quantum states of a bipartite subsystem (A) are entangled when spin, but separable when charge degrees of freedom are under consideration ($N_{\text{el}} = N$), or vice versa ($N_{\text{el}} = N/2$). Such a decoupling should be distinguished from charge–spin separation predicted to appear in 1D systems showing the Luttinger liquid phase [44–47]. Our numerical examples also show there is no one-to-one relation between the decoupling and the Mott transition, as the former can be identified either for the system showing the crossover behavior only or undergoing the Mott transition (in the large- N limit). Finally, the pairwise-entanglement analysis presented above allows one to identify noticeably different behavior of charge and spin correlation functions without referring to their asymptotic behavior, as previously proposed in the literature (see the first paper in [12, 44, 66]).

5. Conclusions

In this study we have demonstrated that pairwise entanglement, quantified by the fermionic concurrence determined separately for charge and spin degrees of freedom, can serve as a convenient indicator for a finite-system version of the Mott transition. In particular, standard finite-size scaling estimates of the Mott transition for linear chains of hydrogenic-like atoms are revisited utilizing the EDABI at the half and the quarter electronic filling. In the latter case, we find that not merely the charge gap indicates the transition for $1/N \rightarrow 0$ (with N being the number of atoms) at the interatomic distance $R_c \approx 4.2 a_0$ (where a_0 denotes the Bohr radius), but also the spin concurrence vanishes for a finite N at $R_*(N)$ taking the values relatively close to R_c . Charge concurrence remains nonzero in both the metallic and the insulating phases, signaling a decoupling between charge and spin degrees of freedom.

At the half filling the Mott transition is not observed. Instead, the crossover from a partly localized quantum liquid to a fully-reconstructed Mott insulator occurs. The charge concurrence vanishes at the crossover point, where the spin concurrence shows a broad peak; the latter remains nonzero in the entire parameter range.

It is worth to stress here that calculations of the fermionic concurrence, employed in this paper, generate essentially no extra computational costs, as the concurrence is determined solely via pairwise ground-state correlation functions for charge or spin degrees of freedom, without referring to the dynamical properties such as the optical or dc conductivity. The analytic relations between entanglement and the correlation functions (see equation (52)) are also derived in this paper.

A striking feature is that the analysis holds true regardless how the exact (or approximated) GS is obtained, making it possible to employ the entanglement-based signatures of the Mott transition when discussing a generic correlated-electron system. What is more, equation (52) also applies when correlation functions on its right-hand side are determined using more powerful numerical techniques, such as DMRG or QMC. For these reasons, we believe the approach we propose may shed new light on various open problems in the field, such as the long-standing metallization of solid hydrogen [4], or the recently-raised phase diagram of the repulsive Hubbard model on a honeycomb lattice ([13], see footnote 1).

Acknowledgments

I thank Andrzej Biborski, Andrzej Kądziaława, and Prof Józef Spałek for many discussions, and Yichen Huang for pointing out the role of asymptotic properties of the reduced density matrix. The work was supported by the National Science Centre of Poland (NCN) via Programme SONATA BIS, Grant No. 2014/14/E/ST3/00256. Computations were performed using the PL-Grid infrastructure.

References

- [1] Schrödinger E 1926 *Phys. Rev.* **28** 1049
- [2] Friedmann T and Hagen C R 2015 *J. Math. Phys.* **56** 112101
- [3] Rycerz A and Spałek J 2004 *Eur. Phys. J. B* **40** 153
Spałek J, Görlich E M, Rycerz A and Zahorbeński R 2007 *J. Phys.: Condens. Matter* **19** 255212
- [4] Kądziaława A P, Bielas A, Acquarone M, Biborski A, Maška M M and Spałek J 2014 *New J. Phys.* **16** 123022
- [5] Kądziaława A P, Biborski A and Spałek J 2015 *Phys. Rev. B* **92** 161101(R)
- [6] Drozdov A P, Erements M I, Troyan I A, Ksenofontov V and Shylin S I 2015 *Nature* **525** 73
- [7] Errea I, Calandra M, Pickard C J, Nelson J, Needs R J, Li Y, Liu H, Zhang Y, Ma Y and Mauri F 2015 *Phys. Rev. Lett.* **114** 157004
- [8] Yazyev O V 2010 *Rep. Prog. Phys.* **73** 056501
Hong J, Bekyarova E, de Heer W A, Haddon R C and Khizroev S 2013 *ACS Nano* **7** 10011
- [9] Prelovšek P and Bonča J 2013 *Strongly Correlated Systems: Numerical Methods* ed A Avella and F Mancini (Berlin: Springer) p 1
- [10] De Chiara G, Rizzi M, Rossini D and Montangero S 2008 *J. Comput. Theor. Nanosci.* **5** 1277
- [11] Sugiyama G and Koonin S E 1986 *Ann. Phys.* **168** 1

- [12] Stella L, Attacalite C, Sorella S and Rubio A 2011 *Phys. Rev. B* **84** 245117
Boguslawski K, Tecmer P, Ayers P W, Bultinck P, De Baerdemacker S and Neck D V 2014 *Phys. Rev. B* **89** 201106(R)
- [13] Sorella S, Otsuka Y and Yunoki S 2012 *Sci. Rep.* **2** 992
Assaad F F and Herbut I F 2013 *Phys. Rev. X* **3** 031010
Otsuka Y, Yunoki S and Sorella S 2016 *Phys. Rev. X* **6** 011029
- [14] Hirsch J E 1985 *Phys. Rev. B* **31** 4403
- [15] Kaplan T A, Horsch P and Fulde P 1982 *Phys. Rev. Lett.* **49** 889
- [16] Yokoyama H and Shiba H 1990 *J. Phys. Soc. Japan* **59** 3669
- [17] Strong S P and Talstra J C 1999 *Phys. Rev. B* **59** 7362
- [18] Yokoyama H, Miyagawa T and Ogata M 2011 *J. Phys. Soc. Japan* **80** 084607
- [19] Zhou S, Wang Y and Wang Z 2014 *Phys. Rev. B* **89** 195119
- [20] Einstein A, Podolski B and Rosen N 1935 *Phys. Rev.* **47** 777
- [21] See review by Bennet C H and Divincenzo D P 2000 *Nature* **404** 247
- [22] Wootters W K 1998 *Phys. Rev. Lett.* **80** 2245
Hill S and Wootters W K 1997 *Phys. Rev. Lett.* **78** 5022
- [23] Osterloh A *et al* 2002 *Nature* **416** 608
- [24] Verstraete F, Martin-Delgado M A and Cirac J I 2004 *Phys. Rev. Lett.* **92** 087201
- [25] van Wezel J, van den Brink J and Zaanen J 2005 *Phys. Rev. Lett.* **94** 230401
- [26] Schliemann J, Loss D and MacDonald A H 2001 *Phys. Rev. B* **63** 085311
- [27] Zanardi P 2002 *Phys. Rev. A* **65** 042101
Zanardi P and Wang X 2002 *J. Phys. A* **35** 7947
- [28] Gu S-J, Deng S-S, Li Y-Q and Lin H-Q 2004 *Phys. Rev. Lett.* **93** 086402
- [29] Wieśniak M, Vedral V and Brukne Č 2008 *Phys. Rev. B* **78** 064108
- [30] Boguslawski K *et al* 2012 *J. Phys. Chem. Lett.* **3** 3129
- [31] Grushin A G, Motruk J, Zaletel M P and Pollmann F 2015 *Phys. Rev. B* **91** 165112
- [32] Oleś A M, Horsch P, Feiner L F and Khaliullin G 2006 *Phys. Rev. Lett.* **96** 147205
- [33] Oleś A M 2012 *J. Phys.: Condens. Matter* **24** 313201
- [34] Chen C C, van Veenendaal M, Devereaux T P and Wohlfeld K 2015 *Phys. Rev. B* **91** 165102
- [35] You W-L, Oleś A M and Horsch P 2015 *New J. Phys.* **17** 083009
You W-L, Horsch P and Oleś A M 2015 *Phys. Rev. B* **92** 054423
- [36] Rycerz A 2006 *Eur. Phys. J. B* **52** 291
- [37] Ramšak A, Mravlje J, Žitko R and Bonča J 2006 *Phys. Rev. B* **74** 241305
Ramšak A and Mravlje J 2008 *Eur. Phys. J. B* **61** 419
- [38] Rycerz A 2008 *Physica B* **403** 1534
- [39] Tooski S B, Buřka B R, Žitko R and Ramšak A 2014 *Eur. Phys. J. B* **87** 145
- [40] Mottet M, Tecmer P, Boguslawski K, Legezab Ö and Reiher M 2014 *Phys. Chem. Chem. Phys.* **16** 8872
Duperroutzel C *et al* 2015 *Chem. Phys. Lett.* **621** 160
- [41] Schliemann J 2013 *New J. Phys.* **15** 053017
Predin S, Wenk P and Schliemann J 2016 *Phys. Rev. B* **93** 115106
- [42] Huang Y 2014 *Phys. Rev. B* **89** 054410
- [43] Czarnik P and Dziarmaga J 2015 *Phys. Rev. B* **92** 035120
Czarnik P and Dziarmaga J 2015 *Phys. Rev. B* **92** 035152
- [44] Sacramento P D, Li Y C, Gu S J and Carmelo J M P 2013 *Eur. Phys. J. B* **86** 507
- [45] Lieb E H and Wu F Y 1968 *Phys. Rev. Lett.* **20** 1445
- [46] Voit J 1993 *J. Phys.: Condens. Matter* **5** 8305
- [47] Berciu M and John S 2000 *Phys. Rev. B* **61** 10015
- [48] Hachmann J, Cardoen W and Chan G K-L 2006 *J. Chem. Phys.* **125** 144101
Lin N, Marianetti C A, Millis A J and Reichman D R 2011 *Phys. Rev. Lett.* **106** 096402
Mazziotti D A 2011 *Phys. Rev. Lett.* **106** 083001
- [49] Spalek J and Rycerz A 2001 *Phys. Rev. B* **64** 161105(R)
Rycerz A and Spalek J 2002 *Phys. Rev. B* **65** 035110
- [50] Hohenadler M, Wessel S, Daghofer M and Assaad F F 2012 *Phys. Rev. B* **85** 195115
- [51] Mermin N D and Wagner H 1966 *Phys. Rev. Lett.* **17** 1133
Hohenberg P C 1967 *Phys. Rev.* **158** 383
- [52] Ejima S, Gebhard F, Nishimoto S and Ohta Y 2005 *Phys. Rev. B* **72** 033101
Sano K and Ohno Y 2007 *Phys. Rev. B* **75** 113103
- [53] Schulz H J 1990 *Phys. Rev. Lett.* **64** 2831
- [54] Meyer J S and Matveev K A 2009 *J. Phys.: Condens. Matter* **21** 023203
- [55] Rycerz A 2003 Physical properties and quantum phase transitions in strongly correlated electron systems from a combined exact diagonalization *ab initio* approach *PhD Thesis* Jagiellonian University th-www.if.uj.edu.pl/ztns/download/phdTheses/Adam_Rycerz_doktorat.pdf
- [56] Blumenstein C, Schäfer J, Mietke S, Meyer S, Dollinger A, Lochner M, Cui X Y, Patthey L, Matzdorf R and Claessen R 2011 *Nat. Phys.* **7** 776
- [57] Mosadeq H and Asgari R 2015 *Phys. Rev. B* **91** 085126
- [58] Capponi S, Poilblanc D and Giamarchi T 2000 *Phys. Rev. B* **61** 13410
- [59] Fano G, Ortolani F, Parola A and Ziosi L 1999 *Phys. Rev. B* **60** 15654
- [60] Biborski A, Kądziaława A P and Spalek J 2015 *Comput. Phys. Commun.* **197** 7
Rycerz K, Tirado-Ramos A, Gualandris A, Portegies Zwart S F, Bubak M and Sloot P M A 2007 *Int. J. High Perform. Comput. Appl.* **21** 210
- [61] Kondo J and Yamaji K 1977 *J. Phys. Soc. Japan* **43** 424
Hubbard J 1978 *Phys. Rev. B* **17** 494
- [62] Burden R L and Faires J D 2011 *Numerical Analysis* (Boston, MA: Brooks/Cole) ch 4

- [63] Resta R 2002 *J. Phys.: Condens. Matter* **14** R625
Resta R and Sorella S 1999 *Phys. Rev. Lett.* **82** 370
- [64] Wootters W K 2001 *Quantum Inf. Comput.* **1** 27
- [65] Eckert K, Schliemann J, Bruss D and Lewenstein M 2002 *Ann. Phys., NY* **299** 88–127
- [66] Gallo-Bueno A, Kohout M and Martín Pendás A 2016 *J. Chem. Theory Comput.* **12** 3053